ACS APPLIED MATERIALS & INTERFACES

Research Article

www.acsami.org

Controlled Microwave-Assisted Growth of Silica Nanoparticles under Acid Catalysis

Derek D. Lovingood,*[,†] Jeffery R. Owens,[‡] Michael Seeber,[§] Konstantin G. Kornev,[§] and Igor Luzinov[§]

[†]Oak Ridge Institute for Science and Education, 4692 Millennium Drive, Ste 101, Belcamp, MD 21017

[‡]Air Force Research Laboratory, Airbase Technology Division, 139 Barnes Drive, Suite #2, Tyndall AFB, Florida 32403, United States

[§]School of Materials Science and Engineering, Clemson University, 161 Sirrine Hall, Clemson, South Carolina 29634, United States

ABSTRACT: In this work, we demonstrate the controlled synthesis of silica nanoparticles as small as 30 nm (±5 nm) and as large as 250 nm (±30 nm) in minutes using surfactant free, microwave-assisted synthetic techniques. Proper choice of solvent, silicic acid precursor, catalyst, and microwave irradiation time were the variables used to control nanoparticle size and, ultimately, overcome the previously reported shortcomings of using microwaves for silica nanoparticle synthesis. In these reactions acetone, a low-tan δ solvent, mediates the condensation reaction, while selective absorption of pulsed microwave radiation by the precursor promotes nanoparticle growth. Dynamic light scattering data, scanning electron micrographs, and transmission electron micrographs of the reaction products show that the size, shape, and granularity of the silica nanoparticles are highly dependent on reaction conditions. These microwave methods have utility for mass production of silica nanoparticles or other nanoparticles by flow-through microwave synthetic methods for industrial applications, as well as a facile method for encapsulating or embedding materials with silica for improved functionality and stability.

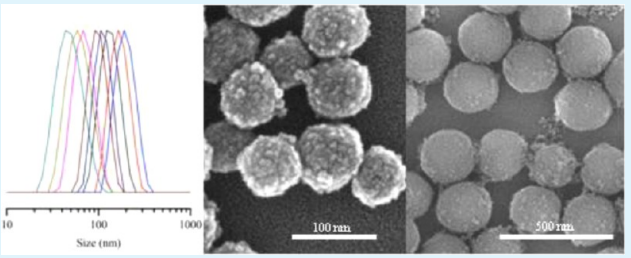

KEYWORDS: *microwave, nanoparticle, silica, silicic acid, NP, SiO_2*

INTRODUCTION

Controlled preparation and growth of functional nanomaterials including semiconductor quantum dots, carbon nanotubes, and metal oxides have received considerable attention in the literature and in industry because of their potential impact in the lucrative areas of electronics, energy production and storage, medicine, and chemical catalysis.[1−13] Specifically, the preparation of silica nanoparticles (SiO_2 NPs) and variants are ideal targets because of silica's transparency to visible wavelengths, dielectric properties, high surface area, ease of functionalization, and relatively low toxicity. These physical properties make silica an attractive material for embedding or encapsulating other materials offering a material with an easily functionalized protective shell.

Although synthesis of nanomaterials remains at the forefront of academic and commercial interest, the breadth, depth, and utility of silicone chemistry regarding the siloxane condensation reactions have been studied for over a century and are still not fully understood. Not surprisingly, such intense academic scrutiny of the area of siloxane chemistry yielded one of the first methods of controlled syntheses of a nanomaterial, now known as the Stöber method. The common methods for preparing SiO_2 NPs include Stöber's method and the water in oil (w/o) reverse microemulsion method.[14] The Stöber and w/o reverse microemulsion methods both involve the hydrolysis and condensation reactions (eqs 1−3) of a siloxane source, typically tetraethyl orthosilicate, catalyzed by mineral acids, ammonia, alkali metal hydroxides, and fluoride containing salts. Methods catalyzed by alkaline conditions typically follow the formation of sols, whereas acid-catalyzed reactions form gels.[15] Variants of both methods include changes in concentration, time, temperature, pH, surfactant, and the use of additional catalyst.[15−24]

$$\equiv Si - OR + H_2O \underset{\text{esterification}}{\overset{\text{hydrolysis}}{\rightleftharpoons}} \equiv Si - OH + ROH \quad (1)$$

$$\equiv Si - OR + HO - Si\equiv \underset{\text{alcoholysis}}{\overset{\text{alcohol condensation}}{\rightleftharpoons}} \equiv Si - O - Si\equiv + ROH \quad (2)$$

$$\equiv Si - OH + HO - Si\equiv \underset{\text{hydrolysis}}{\overset{\text{water condensation}}{\rightleftharpoons}} \equiv Si - O - Si\equiv + H_2O \quad (3)$$

Although eqs 1−3 show the generic equations governing these hydrolysis and condensation, in practice the reaction mechanisms are much more complex and the equilibrium reactions are susceptible to large shifts by minor changes in the local environment of the siloxane precursor. Parameters influencing the nature of the local siloxane environment include: the choice of silicon alkoxide precursor, nature of the catalyst, concentration of silicon alkoxide, $[H_2O]/[TMOS]$

Received: September 17, 2012
Accepted: November 26, 2012
Published: November 26, 2012

ratio, choice of solvent, temperature, and pressure. The length of the alkoxide group of the siloxane precursor directly affects the rate of hydrolysis where methoxy- > ethoxy- > butoxy-. Alkaline catalyzed reactions are commonly favored for SiO_2 NP synthesis, the increased reactivity under alkaline catalysis reactions result in immediate condensation upon hydrolysis whereas stable monomers can be formed using acidic conditions.[25]

SiO_2 NPs have been synthesized by irradiating Stöber reaction solutions at 2.45 GHz using both laboratory microwave reactors and kitchen microwave ovens with limited success or inconsistent results.[20,21,26] The use of microwave ovens and microwave reactors is a rapidly growing area of research in fields ranging from organic chemistry to material science.[27−34] The popularity of microwave-assisted chemistry is not surprising considering these methods often dramatically increase yields, decrease reaction times, and many times allow for solvent-free reactions.[28,35,36] Specifically, syntheses of nanomaterials by microwave-assisted chemical reactions claim advantageous results over conventional heating techniques because they deliver large amounts of controlled power quickly to small volumes of absorbing media, promoting spontaneous nucleation events.[28]

In microwave chemistry, all components of the reaction (reagents, solvents, vessels, etc.) are capable of interacting with or perturbing the electromagnetic field (EM). Molecular species with permanent dipoles align with the electric field and, through these molecular rotations, generate thermal energy (heat) by molecular friction. The dielectric properties of a non-conductive material govern the way it will heat when exposed to microwave radiation, with a combination of ionic conduction and dipole polarization serving as the predominant heating mechanism. The loss factor of a material, tan δ, determines the ability for a specific substance to convert EM energy into heat at a given frequency and temperature. Solvents can be classified according to their loss factor—a high (tan δ > 0.5), medium (0.1 > tan δ > 0.5), and low (tan δ < 0.1) loss factor relates to a solvent's ability to couple with a microwave field and produce heat. Typically, high-loss-factor alcohol solvents (ethanol, 2-propanol or methanol, tan δ = 0.941, 0.799, and 0.659, respectively) have been used in preparation of SiO_2 NPs because a polar solvent is required for solubility for the silicon precursor. For the work described in this paper, these alcohol solvents represent poor choices as they efficiently couple with the EM field, whereas the goal is selective microwave absorption by the reactants. Properly utilizing the benefits of heating with microwaves for driving chemical reactions requires selecting precursor(s) capable of strongly coupling with the EM field and a solvent that minimally interacts with the EM field.

In this manuscript, we describe the controlled microwave-assisted synthesis of SiO_2 NPs by acid-catalysis using tetramethyl orthosilicate (TMOS) in acetone resulting in NPs with diameters ranging from 30 nm up to sizes greater than 250 nm. The reaction conditions are unique since silica condensation is not observed without microwave heating. Through microwave-assisted techniques, growth of colloidal SiO_2 NP *sols* is achieved by acid catalyzed reactions where silica *gels* are typically formed under acidic conditions. SiO_2 NPs are formed by effective coupling of the silicic acid precursor with the EM field where the acetone solvent (tan δ = 0.054) has a minimal role in heating the reaction. The growth of SiO_2 NPs by these microwave-assisted techniques is accurate, precise and quick where reaction times are on the order of seconds to minutes. Control over particle size is achieved by varying the concentration of silicic acid precursor and the duration of exposure of the reaction solution to microwave irradiation. A mechanism for SiO_2 NP formation is proposed for these unique reaction conditions as well as future applications for these techniques.

EXPERIMENTAL SECTION

Chemicals. TMOS, ammonium molybdate hydrate, and concentrated hydrochloric acid were purchased from Sigma−Aldrich (St. Louis, MO). Acetone was purchased from Fisher (Pittsburgh, PA). All water was filtered using a NANOpure water filtration system. All reagents were used without any further purification.

Microwave Synthesis of SiO_2 Nanoparticles. SiO_2 NPs were synthesized in a single-mode 2.45-GHz CEM Discover SP microwave reactor capable of producing 300 W. For a typical microwave reaction in the CEM reactor, a water-soluble microwave reactive silicon species, silicic acid, is prepared by the hydrolysis of TMOS using 1 mM HCl, 15% TMOS by volume. The silicic acid solution is then diluted with acetone by volumetric ratios of silicic acid to acetone, 1:66, 1:50, 1:40, 1:33, 1:28, 1:25, 1:22, 1:20. Once the mixture is prepared, 5 mL aliquots are placed in a 10 mL CEM vial containing a stir bar and snap cap. A reaction temperature of 125 °C is reached after ∼70 s of ramping the reaction solution at 300 W. After reaching 125 °C, a maximum pressure of ∼74 psi and average power of ∼65 W are maintained for 60 s (times are varied for time dependent reactions). Reaction solution temperatures are measured externally using an IR thermometer.

Characterization. SiO_2 NPs were measured by dynamic light scattering (DLS) using a Malvern Zetasizer Nano90 to quickly interrogate differences between separate reactions. Serial dilutions of the reaction solution were performed with acetone and water to ensure particle aggregation is limited when sizing. Aliquots for DLS measurements were prepared by mixing 100 μL aliquots of sample in 1 mL of solvent in 1 cm quartz cuvettes. The reported DLS size results are determined by intensity measurements. Zeta potentials were measured in disposable folded capillary cells. Reaction solutions for zeta potential were analyzed as "as prepared" and "cleaned" solutions. Protocals for cleaning include centrifugation of the NP suspensions (Eppendorf Minispin Plus) at 14 500 rpm for 60 min, decanting and resuspending fresh acetone (3×). Water was used for a solvent for measuring zeta potentials of both "as prepared" and "cleaned" solutions.

Scanning Electron Microscopy. SiO_2 NPs were imaged by scanning electron microscopy (SEM) to examine the morphology and to measure the average diameter of the NPs. SEM were conducted using a Hitachi S4800 field emission scanning electron microscope. Highly polished single-crystal silicon wafers (Semiconductor Processing Co.) were cleaned in an ultrasonic bath for 30 min, placed in a hot (80 °C) "piranha" solution (3:1 conc. H_2SO_4−30% H_2O_2) for 1 h, and then rinsed several times with high-purity DI water. "Cleaned" suspensions were drop-cast onto clean silicon wafers prior to imaging. All NP samples were sputter-covered with platinum for 1 min before imaging.

Transmission Electron Microscopy. SiO_2 NPs were imaged by transmission electron microscopy (TEM) to further examine the nature of the surface of the materials. The morphology of the synthesized particles was inspected using a Hitachi H-9500 transmission electron microscope (TEM). "Cleaned" suspensions were mounted from a suspension in acetone onto a copper grid for imaging.

Molybdenum Complexation UV−Vis Study. Molybdenum complexation studies were performed using literature precedence[37] to measure the concentration of silicic acid monomers present in solution of before and after microwave heating. A molybdic acid solution was prepared using 2 g of ammonium molybdate hydrate and 6 mL of concentrated HCl and diluting with water to 100 mL. A working solution was prepared by diluting 1.5 mL of the molybdic acid in 15 mL of water. Aliquots (5−100 μL) of the reaction solution

containing silicic acid were added to the working solution and allowed to equilibrate for 15 min before analysis by UV−vis. The formation of the silico-molybdate species was indicated by solution turning yellow after a few seconds of injection of the silicic acid reaction solution. The concentration of silico-molybdate species was determined by UV−vis at a wavelength of 410 nm. Repeated scans of each solution were performed to ensure the concentration of the silico-molybdate complex did not change over the course of the experiment.

RESULTS AND DISCUSSION

Controlled Growth of Silica by Microwave Pulses. The microwave-assisted methods presented produce SiO_2 NPs quickly, effectively, repeatedly and over a range of sizes. While techniques such as UV−vis or photoluminescence are commonly used for quick interrogation of size in nanomaterials, the transparent nature of SiO_2 limits the value of these optical techniques and requires the employment of alternative methods. Dynamic light scattering (DLS) offers the ability to quickly and easily measure the average particle size between each reaction. The ability to accurately control the growth of SiO_2 NPs through sizes ranging from 30 to 250 nm using these synthetic methods is illustrated through DLS measurements in Figure 1a and b. In Figure 1a, DLS size data of SiO_2 NP where incremental growth is observed by sequentially increasing the initial concentration of TMOS. All reactions were prepared under similar conditions; 5 mL acetone solvent and microwave irradiation at 125 °C for 60 s. Changing the initial concentration of TMOS allowed for controlled incremental growth of SiO_2 NPS with sizes measured by DLS equivalent to diameters of 56, 82, 125, 150, 194, 227, 264, and 273 nm (Figure 1b).

In Figure 1c, the precision of this synthetic technique is illustrated through the repeated growth of SiO_2 NPs with targeted diameters of ∼50 and ∼200 nm. For the smaller SiO_2 NPs five separate reactions yielded particles with an average DLS size of 57 ± 4 nm, whereas for the larger SiO_2 NPs, six separate reactions yielded SiO_2 NPs with an average diameter of 212 ± 15 nm. SiO_2 NPs with average diameters of 57 ± 4 nm were prepared using 25 mM concentration of TMOS and irradiating to 125 °C for 10 s, whereas the larger particles were prepared using 50 mM of TMOS and irradiating to 125 °C for 30 s. These data demonstrate the high degree of precision and accuracy afforded by this technique for synthesizing SiO_2 NPs by manipulation of only two variables, irradiation time and TMOS concentration.

Although DLS quickly differentiates between the separate SiO_2 NP reactions, DLS does not provide evidence to the overall uniformity or quality of the synthesized material. In Figure 2, SEM images illustrate the shape and uniformity of the SiO_2 NPs grown by varying the concentration represented through DLS data in Figure 1a. The average diameters for the series of SiO_2 NPs (Figure 2a−h) measure 48 ± 4, 70 ± 7, 101 ± 10, 127 ± 12, 164 ± 15, 189 ± 19, 206 ± 21, and 224 ± 30 nm. The SEM images show that the NPs are spherical with a roughened surface morphology for all sizes. Note the rough surface as well as the appearance of deposits of isolated, amorphous debris is atypical compared to particles made by traditional alkaline catalyzed Stöber methods. As it is most prevalent in reactions with high silicic acid precursor concentration, the amorphous material is likely randomly deposited silica that condenses from silicic acid precursor remaining in solution after the microwave heating step. In Figure 3, the average SiO_2 NP size measured by SEM is plotted vs. TMOS concentration and the linear trend observed is consistent with the DLS data. These linear results from the SEM support the conclusion that these techniques result in the controlled growth of SiO_2 NPs. Further, the SEM data corroborates the DLS data and validates the use of DLS as a reasonably accurate tool for monitoring particle size between these reactions.

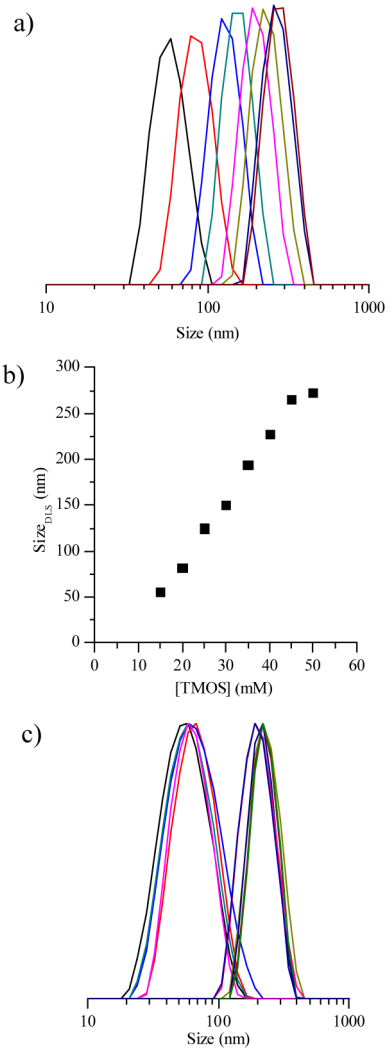

Figure 1. (a) Accuracy in SiO_2 NP as a result of change in concentration of TMOS. Sizes range from 56−273 nm in diameter. TMOS concentration =15 (black), 20 (red), 25 (blue), 30 (teal), 35 (pink), 40 (olive), 45 (d. blue), and 50 mM (garnet). (b) Linear dependence of particle size vs. TMOS concentration. (c) Precision of SiO_2 NP growth where average peak sizes are 57 ± 4 and 212 ± 15 nm.

Time Dependence on SiO_2 NP Growth. A time-dependent study of this technique reveals that microwave irradiation time also allows limited control of surface roughness and shape of the NPs. For this experiment series (Figure 4a), five separate reactions with initial concentrations of TMOS equal to 25 mM were irradiated at 125 °C for 5, 15, 30, 45, and 60 s. For the 25 mM series, the diameters of SiO_2 NPs measured by DLS are 69, 78, 102, 103, and 106 nm. In Figure 4b, seven separate reactions with initial concentrations of TMOS equal to 50 mM were irradiated at 125 °C for 5, 15, 30, 45, 60, 75, and 90 s. For the 50 mM series, the diameters of

dx.doi.org/10.1021/am3020247 | ACS Appl. Mater. Interfaces 2012, 4, 6875−6883

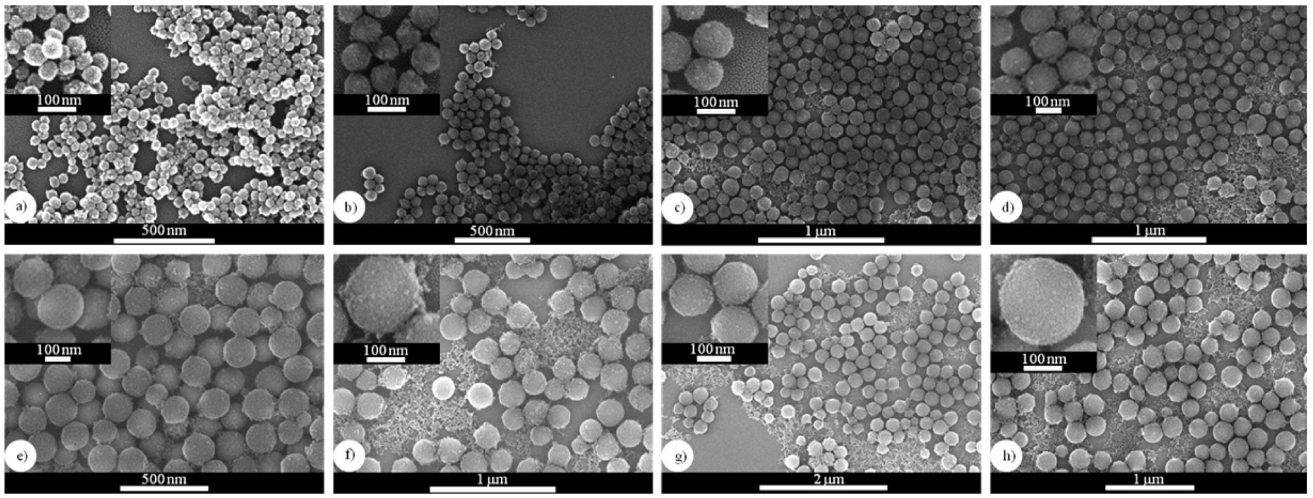

Figure 2. SEM images of SiO_2 NPs grown by increasing initial concentration of TMOS. Initial concentration of TMOS equals (a) 15, (b) 20, (c) 25, (d) 30, (e) 35, (f) 40, (g) 45, and (h) 50 mM. Roughened surfaces are atypical compared to traditional Stöber NPs.

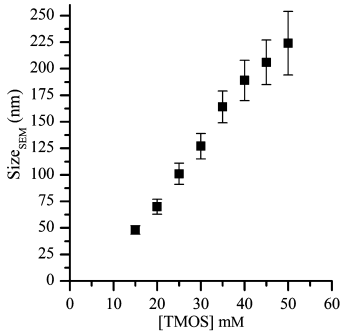

Figure 3. Linear dependence of SiO_2 NP size measured by SEM. Trend is consistent to linear trend observed in DLS.

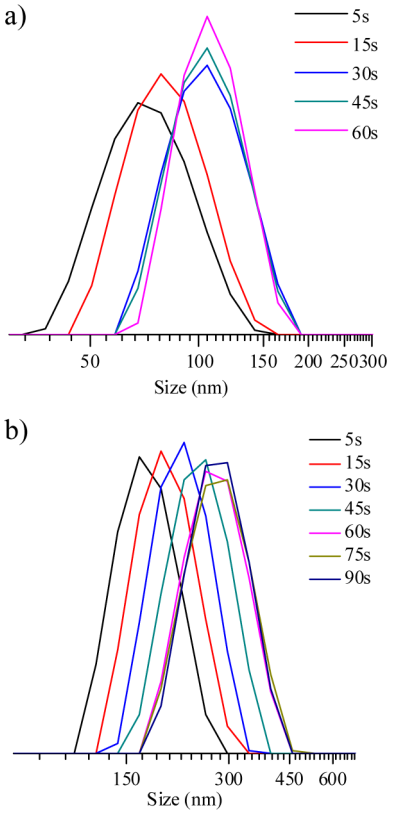

Figure 4. Time dependence of SiO_2 NP growth measured by DLS. TMOS precursor concentration = (a) 25 and (b) 50 mM. Time points are listed in each plot. Minimal growth in particle size is observed for the 25 mM reaction between 30 and 60 s and 60 and 90 s for the 50 mM series.

SiO_2 NPs measured by DLS are 169, 192, 217, 239, 268, 274, and 273 nm.

In Figure 5a, SiO_2 NPs grown with a reaction time of 5 s have irregular asymmetric shape, rough surfaces and an average particle size is 29 ± 6 nm. In Figure 5b, the reaction time is increased to 10 s and the SiO_2 NPs are slightly more symmetric, but still have rough surfaces. Average particle diameters have increased to 40 ± 5 nm for the particles in Figure 5b. In Figure 5c, symmetrical SiO_2 NPs with an average diameter of 72 ± 7 nm were prepared by increasing the reaction time to 60 s. These particles still have rough surfaces which is consistent for all the particles grown by these methods. The degree of surface roughness and asymmetric shape seems most pronounced for shorter reaction times with a pronounced increase in spherical shape with retention of surface roughness for longer reaction times. The increase in spherical shape with reduction, but marked retention of surface roughness compared to traditional methods suggest that Ostwald ripening is likely not the primary synthetic mechanism for particle formation and suggest a degree of self-assembly associated with the longer irradiation times.

To illustrate the overall trend from the results of the time dependent experiment, the peak sizes measured by DLS for both series are plotted against microwave irradiation time in Figure 6. The 25 mM series shows a linear trend in particle size when reaction times are between 5 and 30 s, whereas reaction times greater than 30 s show minimal or no growth—the average particle diameter for the 30, 45, and 60 s reactions was 104 ± 2 nm. These results suggest the majority of silicic acid precursor is consumed within 30 s of reaction time for this concentration. Similarly, the 50 mM series shows a linear trend in particle size for reaction times between 5 and 60 s, whereas reaction times greater than 60 s result in minimal change in particle size—the average particle diameter for the 60, 75, and 90 s reactions was 272 ± 3 nm. The DLS data show that once a minimum irradiation interval is reached, growth in the SiO_2

dx.doi.org/10.1021/am3020247 | ACS Appl. Mater. Interfaces 2012, 4, 6875−6883

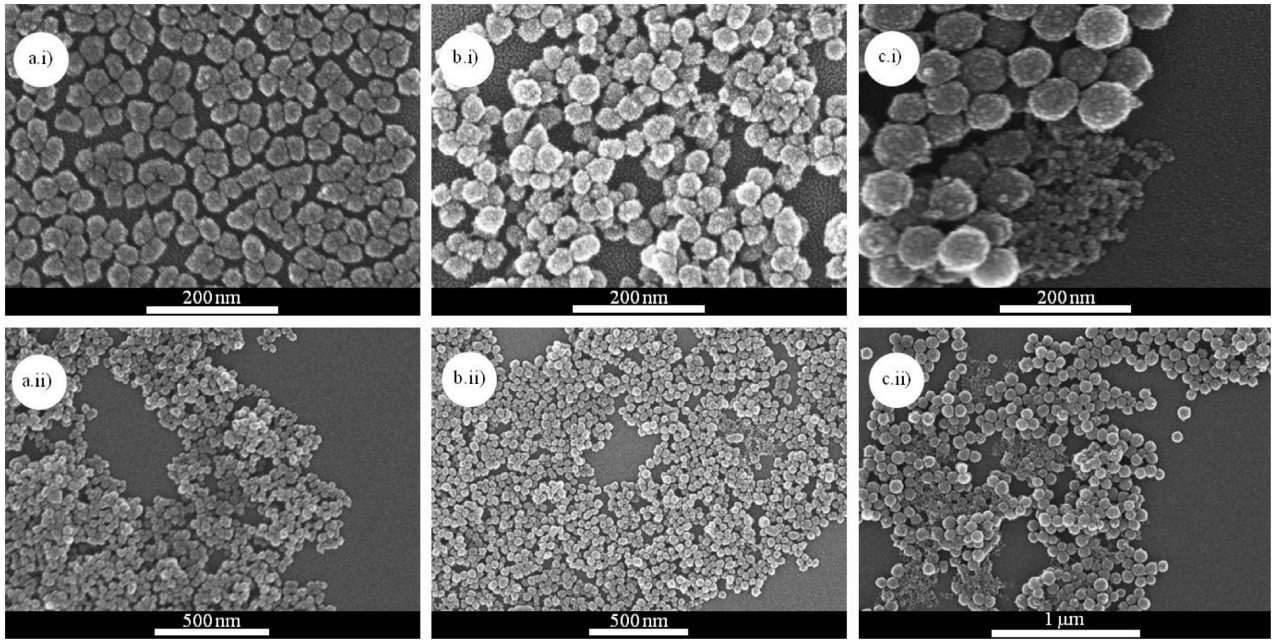

Figure 5. SEM images of SiO_2 NPs grown by time dependent reactions. NP diameters are (a) 29 ± 6 nm, (b) 40 ± 5 nm, and (c) 72 ± 7 nm. SiO_2NPs grown with shorter reaction times (≤30 s) are irregular in shape and have rough surfaces.

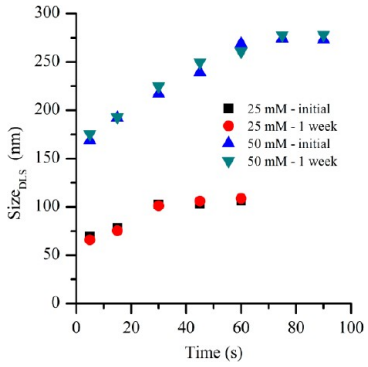

Figure 6. Plot of DLS peak size vs time for the 25 and 50 mM series. A linear trend in particle size is observed for both concentrations until particle growth stalls. Reaction solutions were also sized 1 week later to observe any change in particle size due to residual precursor.

NPs is not observed (Figure 4), although smoother more spherical particles are formed (Figure 5).

DLS measurements showed the reaction solution to be stable for weeks with no evidence of condensation of the silica material. Resizing the SiO_2 NPs from the time dependent experiment (Figure 4) using DLS one week after the initial sizing revealed minimal change in mean particle size (Figure 6). An average change of 3.1 ± 1.4% in particle size was observed for the 25 mM series and an average change of 2.7 ± 1.4% was observed for the 50 mM series. The minimal change in SiO_2 NP size measured between the time periods indicates the synthesis of SiO_2 NPs from TMOS in acetone under acid catalysis is driven by microwave irradiation and further supports the conclusion that the mechanism of particle formation is fundamentally different from traditional Ostwald ripening driven Stöber syntheses.

Surface Characterization. TEM microscopy was performed on select SiO_2 NPs previously imaged by SEM (Figure 2a, e, and h) to further investigate the nature of the rough surface apparent by SEM (Figures 2 and 5). Figure 7 shows TEM images with average diameters of SiO_2 NPs measuring 49 ± 5 nm in diameter (a), 163 ± 13 nm in diameter (b), and 238 ± 26 nm in diameter (c). These TEM mean diameter values agree with corresponding SEM measured values illustrated in Figure 2. The TEM images reveal that the particles in Figure 7a appear truncated with flat surfaces and have polyhedron shape, whereas particles in Figure 8b,c have smoother surfaces compared to those in Figure 7a, but some surface distortion is observed. From SEM and TEM images none of the products imaged to date possess the smooth surface that is indicative of traditional Stöber particles produced by alkaline-catalyzed methods.

Zeta potentials were performed on the SiO_2 NPs in "as prepared" and "cleaned" in water to determine the degree of particle stability. The "as prepared" samples measured zeta potentials of −15.4 ± 0.3 mV. The "cleaned" samples measured zeta potentials of −30.0 ± 1.7 mV. These results suggest that the removal of residuals from the reaction solution can increase particle stability by the formation of a stable water monolayer.

Efficiency of Conversion of Silicic Acid by Microwave Heating. Molybdenum complexation assays were performed to determine the effective rate of conversion of the silicic acid precursor to colloidal SiO_2 NPs under microwave heating. Stoichiometrically, only one silicic acid monomer will bind in the formation of the silico-molybdate species. The complex species is yellow in color in solution and its concentration can be measured by UV−vis, thus the concentration of silicic acid monomers can be determined. Unfortunately, the molybdate will only bind to monomers of silicic acid thus dimers, trimers or larger oligomers cannot be detected.

In Figure 8, three silico-molybdate traces are presented where the traces represent a solution before exposure of microwaves and solutions where SiO_2 NPs were formed under microwave heating with initial TMOS concentrations of 25 and 50 mM. The individual points in Figure 8 are the concentration of the silico-molybdate at 410 nm. All three traces show a linear dependence with increasing volume of the reaction solution

dx.doi.org/10.1021/am3020247 | ACS Appl. Mater. Interfaces 2012, 4, 6875−6883

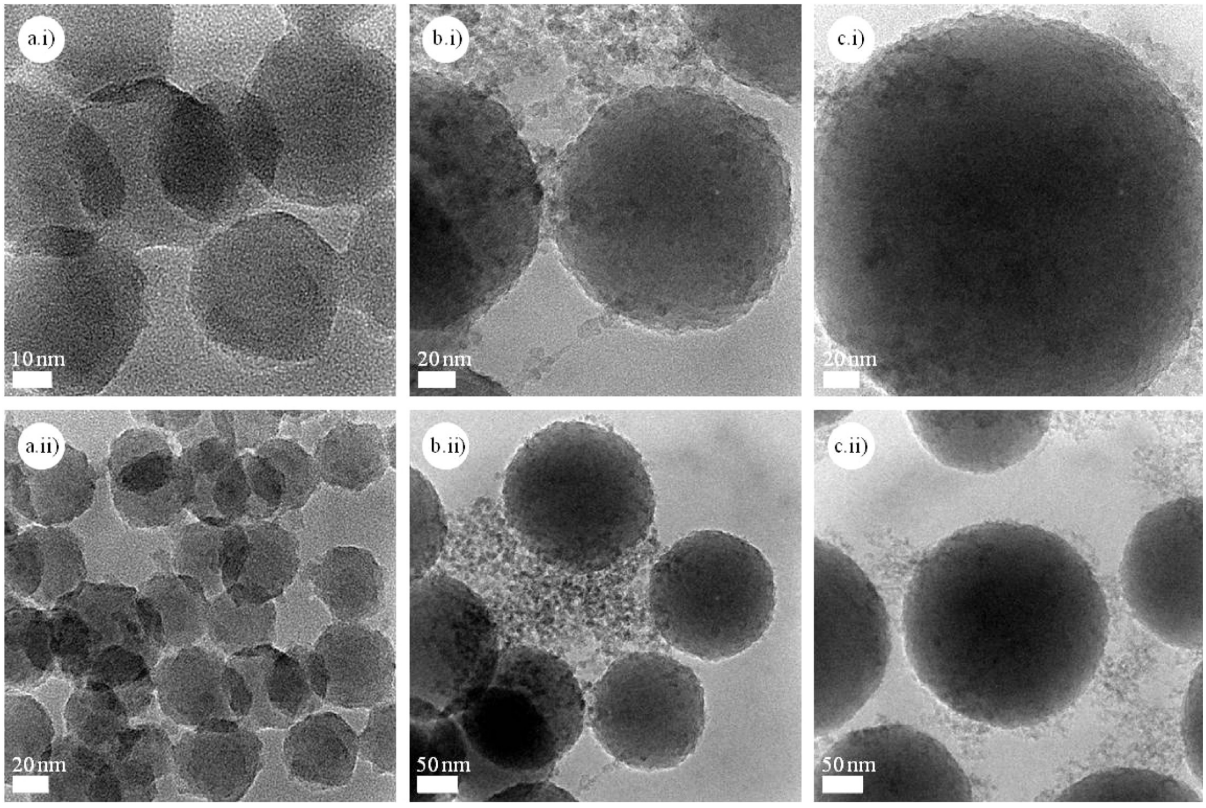

Figure 7. High-resolution TEM images of SiO_2 NPs synthesized by microwave-assisted methods. (a) Evidence of nonspherical NPs is observed for particles with diameters of 49 ± 5 nm. Particles appear to be polyhedron in shape. (b, c) Spherical SiO_2 NPs are observed for the larger particles. Particles imaged in b have average sizes of 163 ± 13 nm, whereas particles in c have average sizes of 238 ± 26 nm.

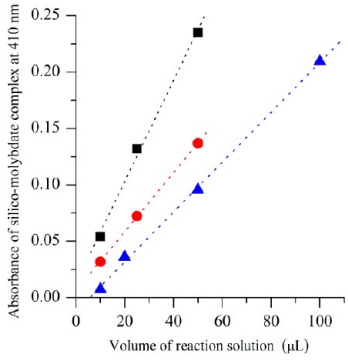

Figure 8. Silico-molybdate complex species measured by UV−vis at 410 nm. Black square = pre-microwave solution. Blue triangle = 25 mM and red circle = 50 mM after exposure to microwave irradiation for 60s at 125 °C. Linear fits are added to help visualize overall trend in data.

containing silicic acid providing a means to determine the relative conversion of silicic acid to colloidal SiO_2 NPs. Assuming the pre-microwave trace in Figure 8 represents a solution containing the highest possible concentration of silicic acid monomer, relative conversion rates of silicic acid to colloidal SiO_2 NPs can be determined for the reactions where colloidal SiO_2 NPs are produced through microwave heating. Monomer concentration should be greatest immediately after hydrolysis of the TMOS and should be stable in the pre-microwave solution because the particle growth was not observed without microwave heating (Figure 6).

Analysis of the change in slope for the separate traces in Figure 8 provides a means to determine the relative rate of precursor conversion. The slope for the pre-microwave trace is 4.48×10^{-3} with a R^2 value of 0.9959, where the slopes for the 25 and 50 mM traces are 2.62×10^{-3} (R^2 = 0.9998) and 2.21×10^{-3} (R^2 = 0.9986), respectively. Comparing 25 mM and the pre-microwave slopes, the relative amount of silico-molybdate remaining after microwave heating is determined to equal 58% equating to a 42% conversion of silicic acid to colloidal SiO_2 NP for the 25 mM reaction. The relative amount of silico-molybdate remaining in the 50 mM sample after microwave heating was determined to be 49% equating 51% conversion of silicic acid to colloidal SiO_2 NP. The 50 mM reaction is believed to have a higher rate of conversion because the available precursor capable to couple with the EM field is greater resulting in quicker growth kinetics for this concentration. The presence of the yellow silico-molybdate species in the microwave irradiated samples as measured by UV−vis suggests the positive presence for residual silicic acid monomer after microwave heating and incomplete conversion for the reactions. These results are contradictory to results observed in the DLS data showing linear dependence then minimal growth (Figures 4 and 6). The residual monomers present in solution explain the presence of the random condensed silica in the SEM (Figures 2 and 5) and TEM (Figure 7). This residual silicic acid is responsible for the formation of amorphous silica and condenses as the solvent evaporates in preparation of samples for imaging even with the cleaning procedures employed.

Proposed Mechanism for Growth. On the basis of these reaction parameters, these conditions support a mechanism for SiO_2 NPs formation by acid catalyzed microwave-assisted reactions which include the formation of a stable pre-

dx.doi.org/10.1021/am3020247 | ACS Appl. Mater. Interfaces 2012, 4, 6875−6883

microwave reaction solution and condensation driven by microwave heating. Once the siloxane source hydrolyzes, monomers form which leads to the formation of oligomers that polymerize and depolymerize (eqs 2−3) resulting in the formation of larger silica networks. Control over the reaction conditions is critical in the overall formation of the type of silica network, sol or gel, produced. Note that under acid catalysis; siloxane condensation reactions typically yield gels, not colloidal sols as produced under these microwave-assisted method. The formation of colloidal sols can be favored if conditions for depolymerization are present, which allows restructuring of the growing material.[38] As stated previously, eqs 1−3 represent highly simplified equilibrium equations that summarize the hydrolysis and condensation reactions where the siloxane source is susceptible to changes in its local chemical environment. In our microwave-assisted reaction, the key parameters governing the reaction conditions include: TMOS as the silicon alkoxide, 1 mM HCl as the catalyst, μmol concentrations of TMOS, $[H_2O]/[TMOS]$ ratio of 46/1, acetone as a solvent, and elevated temperatures and pressures. The key parameters governing the reaction can increase the stabilization of reaction intermediates, such as silica octamers or transition states, such as pentacoordinate and hexacoordinate silanes.[25,38,39] Recently, a DFT study has postulated that the formation of stable silica intermediates and transition states are possible when acidic conditions and high $[H_2O]$ conditions are met. These intermediates and transition states are stabilized by the elongation of the hydroxyl bonds and siloxane bonds.[39]

This body of data indicates our pre-microwave reaction solution is stable, consisting primarily of silicic acid monomers. This conclusion is supported by the molybdate assays, which confirm high concentrations of silicic acid monomers in the pre-microwave solution and absence of any condensed material after days confirming solution stability. Note that this conclusion is also supported in the literature, as acetone is known to retard the silicic acid condensation reaction and, through solvation stabilizes the silicic acid monomer.[25] Upon microwave irradiation of the reaction solution, reasonably monodisperse SiO_2 NPs form, with the size being dependent on silicic acid precursor concentration and the shape and morphology dependent on irradiation time. Condensation of colloidal SiO_2 sols under acid catalysis occurs by microwave heating, which results from coupling of the silicic acid precursor with the microwave field. On the basis of our reaction conditions, condensation of silicic acid to colloidal SiO_2 NPs is predominately driven by the water condensation reaction since unhydrolyzed variants of the TMOS precursor are minimal. The condensation reaction could also be assisted by the pressure generated during the reaction because of the superheating of the solvent, as increased pressures have been shown to increase the rate of polycondensation within silica species.[40] Note that controlled SiO_2 NP growth under these conditions has not been reported previously in the literature to our knowledge. From the observed stall in particle growth and appearance of silicic acid monomer from the molybdate assays, the presence of a self-limiting growth mechanism may be responsible for particle growth and the smoothing of the particle surface. The fact that independent of NP size, extended irradiation times continue to affect the NP surface morphology and shape, even after NP growth has stabilized, indicates that microwave irradiation continues to drive the polymerization-depolymerization reaction. The observation that extended irradiation of NP leads to smoother and more spherical particles indicates that smoother more spherical particles are thermodynamically favored under microwave irradiation.

In SEM images shown in Figure 5, irregular shaped particles are observed at short reaction times (<30 s) and more spherical shaped particles at longer reaction times (≥30 s). This observation suggest that extended reaction times result in annealing and rearrangement of the particle surface to higher ordered, symmetrical particles. With longer reaction times, silicic acid monomers can polymerize and depolymerize on and off the surface creating more spherical particles. This polymerization growth process is driven by microwave heating and depolymerization is driven by the unique reaction conditions. Synthesis of small (20−50 nm) spherical SiO_2 NPs using microwave-assisted acid catalysis requires a balance of irradiation time and silicic acid precursor concentration (Figure 2a vs 5a). These observations are consistent with the physics of microwaves influencing molecular interactions. Reductions in the degrees of freedom of movement of a molecule equate to reductions in the molecule to oscillate and interact with the EM field. Silicic acid monomers that have >1 bonds to the silica matrix will reduce its ability to both depolymerize and oscillate with the field. A classic example of this type of behavior can be observed in a cube of ice as it is heated in the microwave. Upon microwave heating, the inner crystalline water of the cube does not heat where the outer surface defects and edges do heat. This heating is due to a higher degree of freedom of the water molecules at the surface and more mobile water molecules at edges, which leads to the cube slowly melting as a sphere. Our reaction conditions further facilitate this behavior as we employ a solvent, acetone, that has minimal interaction with the EM field, thus ensuring maximum microwave field coupling with the silicic acid monomer and with the NP surface defects and edges.

Applications for Microwave-Assisted SiO_2 NP. As previously mentioned, silica is a material of great interest for use in applications such as drug delivery and sensors due to silica being a highly transparent dielectric material with high surface areas capable of being easily functionalized and having low toxicity. The microwave-assisted methods presented provide a method to quickly and reproducibly synthesize SiO_2 NPs of varying diameters as well as a method to encapsulate other substrates.

One of the goals for the Department of Defense is the development of materials that will increase individual protection of garments for military personal while simultaneously reducing the thermal burden. Protective coatings have been developed[41] that provide an excellent protection against liquids but fail in the protection of vapors. The incorporation of SiO_2 NPs into the protective coating offers a means to develop a garment capable of protecting against vapors as well as liquids. The increase in observed protection comes with nominal increase in the weight of the fabric. In Figure 9, SEM microscopy illustrates a cotton fiber containing SiO_2 NPs bound in a protective coating. Initial studies show the incorporated SiO_2 NPs increase the level of protection by preventing chemical simulants for VX from passing through the material. Studies are ongoing on the characterization and the efficiency of the coating including SiO_2 NPs. Although this application is specifically targeted for increasing individual protection for military purposes, the incorporation of SiO_2 NPs or other nanomaterials into coatings by these microwave techniques could be of use in the development of filters for removing particular species in filtration systems.

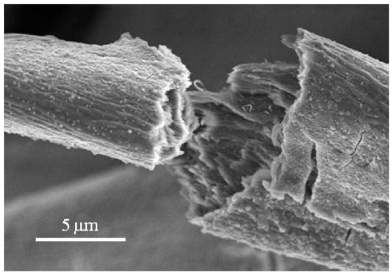

Figure 9. SEM of cotton fibers coated with a protective coating containing SiO_2 NPs. The SiO_2 NPs were synthesized using techniques described in the manuscript. The application of the protective coating containing the SiO_2 NPs was applied by microwave techniques and will be described in detail in a future manuscript.

To further illustrate the utility of these microwave-assisted methods, the encapsulation of other substrates such as CdSe quantum dots with silica is possible. The growth of a silica shell on a substrate such as CdSe quantum dot can provide a layer of protection against oxidation, a material soluble in aqueous media, and a material with a surface that can be easily functionalized. By modifications of the procedure in this manuscript, CdSe/ZnS/SiO_2 QDs can be prepared where the quantum efficiency of the material is maintained and a water-soluble material is produced. Through similar methods used to encapsulate SiO_2 NPs onto cotton fibers Figure 9, CdSe/ZnS/SiO_2 particles are bound to cotton fibers by microwave-assisted methods. In Figure 10, fluorescent microscopy images of cotton

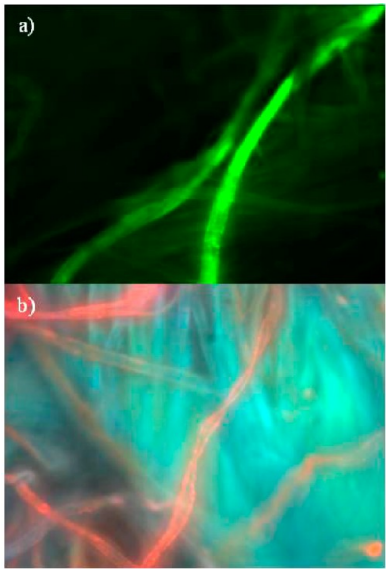

Figure 10. Fluorescent microscopy images of CdSe/ZnS/SiO_2 bound to cotton fibers through a coating applied via microwave assisted techniques. QDs have a wavelength of emission of (a) 525 and (b) 625 nm. Detailed descriptions of the procedure will be in a future manuscript.

fibers containing CdSe/ZnS/SiO_2 bound to the surface of the fiber in a silica coating. The quantum dots maintain their emissive properties while bound to the cotton substrate and emit at (a) 525 and (b) 625 nm, respectively. The ability to control the surface coverage of quantum dots on the fibers is currently being investigated as well as controlling the thickness of the silica shell. Coating substrates such as quantum dots with silica provides a water-soluble, functional material with applications for sensors and several biorelated applications.

CONCLUSION

In this manuscript, we demonstrate novel, surfactant-free, microwave-assisted synthetic methods for precise and accurate synthesis of SiO_2 NPs ranging from 30 to 250 nm. Reaction conditions, product characterization, and molybdate assay data suggest a self assembly synthetic mechanism driven by microwave-dependent polymerization-depolymerization processes and that the reaction does not proceed through the typical Ostwald ripening driven Stöber method. Acetone both stabilizes the silicic acid monomer in the reaction solution and allows strong coupling of the microwave field with the reactants. Depolymerization reactions are facilitated by the reaction conditions which include the use of acetone, high [H_2O]/[TMOS], and choice of acid catalysis. Silicic acid concentration serves to control particle size, and microwave irradiation intervals provide limited control of NP shape and surface morphology. These microwave methods have utility for mass production of SiO_2 NPs or other NPs by flow-through microwave synthetic methods for industrial applications, as well as a quick method for encapsulating material with silica for improved functionability. Further studies are ongoing, investigating the effects on growth of SiO_2 NPs due to the addition of additional catalyst to the reaction.

AUTHOR INFORMATION

Corresponding Author

*E-mail: derek.lovingood.ctr@us.af.mil.

Notes

The authors declare no competing financial interest.

ACKNOWLEDGMENTS

Funding was provided by the Defense Threat Reduction Agency, Physical Science and Technology Division, Protection and Hazard Mitigation technical area. This research was supported in part by an appointment to the Postgraduate Research Participation Program at the Air Force Research Laboratory administered by the Oak Ridge Institute for Science and Education (ORISE) through an interagency agreement between the U.S. Department of Energy and the Air Force Research Laboratory, Materials and Manufacturing Directorate, Airbase Technologies Division (AFRL/RXQ).

REFERENCES

(1) Sorensen, L.; Strouse, G. F.; Stiegman, A. E. *Adv. Mater.* **2006**, *18*, 1965.
(2) Tachikawa, T.; Fujitsuka, M.; Majima, T. *J. Phys. Chem. C* **2007**, *111*, 5259.
(3) Lita, A.; Washington, A. L.; van de Burgt, L.; Strouse, G. F.; Stiegman, A. E. *Adv. Mater.* **2010**, *22*, 3987.
(4) Shen, J. H.; Zhu, Y. H.; Yang, X. L.; Li, C. Z. *Chem. Commun.* **2012**, *48*, 3686.
(5) Kamat, P. V. *J. Phys. Chem. C* **2008**, *112*, 18737.
(6) Mora-Sero, I.; Gimenez, S.; Fabregat-Santiago, F.; Gomez, R.; Shen, Q.; Toyoda, T.; Bisquert, J. *Acc. Chem. Res.* **2009**, *42*, 1848.
(7) Medintz, I. L.; Uyeda, H. T.; Goldman, E. R.; Mattoussi, H. *Nat. Mater.* **2005**, *4*, 435.
(8) Yin, Y.; Alivisatos, A. P. *Nature* **2005**, *437*, 664.
(9) Chan, W. C. W.; Maxwell, D. J.; Gao, X. H.; Bailey, R. E.; Han, M. Y.; Nie, S. M. *Curr. Opin. Biotechnol.* **2002**, *13*, 40.
(10) Halas, N. J. *ACS Nano* **2008**, *2*, 179.
(11) Tang, F. Q.; Li, L. L.; Chen, D. *Adv. Mater.* **2012**, *24*, 1504.

(12) Wang, Y. J.; Price, A. D.; Caruso, F. *J. Mater. Chem.* **2009**, *19*, 6451.
(13) Guerrero-Martinez, A.; Perez-Juste, J.; Liz-Marzan, L. M. *Adv. Mater.* **2010**, *22*, 1182.
(14) Arriagada, F. J.; Osseo-Asare, K. *J. Colloid Interface Sci.* **1999**, *211*, 210.
(15) Chen, S. L.; Dong, P.; Yang, G. H.; Yang, J. J. *Ind. Eng. Chem. Res.* **1996**, *35*, 4487.
(16) Chiang, Y. D.; Lian, H. Y.; Leo, S. Y.; Wang, S. G.; Yamauchi, Y.; Wu, K. C. W. *J. Phys. Chem. C* **2011**, *115*, 13158.
(17) Hartlen, K. D.; Athanasopoulos, A. P. T.; Kitaev, V. *Langmuir* **2008**, *24*, 1714.
(18) Finnie, K. S.; Bartlett, J. R.; Barbe, C. J. A.; Kong, L. G. *Langmuir* **2007**, *23*, 3017.
(19) El Hawi, N.; Nayral, C.; Delpech, F.; Coppel, Y.; Cornejo, A.; Castel, A.; Chaudret, B. *Langmuir* **2009**, *25*, 7540.
(20) Mily, E.; Gonzalez, A.; Iruin, J. J.; Irusta, L.; Fernandez-Berridi, M. J. *J. Sol−Gel Sci. Technol.* **2010**, *53*, 667.
(21) Park, S. E.; Kim, D. S.; Chang, J. S.; Kim, W. Y. *Catal. Today* **1998**, *44*, 301.
(22) Qiao, Z. A.; Zhang, L.; Guo, M. Y.; Liu, Y. L.; Huo, Q. S. *Chem. Mat.* **2009**, *21*, 3823.
(23) Yu, Q. Y.; Wang, P. P.; Hu, S.; Hui, J. F.; Zhuang, J.; Wang, X. *Langmuir* **2011**, *27*, 7185.
(24) Zhang, J. C.; Liu, M.; Zhang, A. F.; Lin, K. F.; Song, C. S.; Guo, X. W. *Solid State Sci.* **2010**, *12*, 267.
(25) Iler, R. K. *The Chemistry of Silica— Solubility, Polymerization, Colloid and Surface Properties and Biochemistry*; Plenum Press: New York, 1979.
(26) Davies, G. L.; Barry, A.; Gun'ko, Y. K. *Chem. Phys. Lett.* **2009**, *468*, 239.
(27) Caddick, S.; Fitzmaurice, R. *Tetrahedron* **2009**, *65*, 3325.
(28) Baghbanzadeh, M.; Carbone, L.; Cozzoli, P. D.; Kappe, C. O. *Angew. Chem., Int. Ed.* **2011**, *50*, 11312.
(29) Tompsett, G. A.; Conner, W. C.; Yngvesson, K. S. *ChemPhysChem* **2006**, *7*, 296.
(30) Lovingood, D. D.; Strouse, G. F. *Nano Lett.* **2008**, *8*, 3394.
(31) Washington, A. L.; Strouse, G. F. *Chem. Mater.* **2009**, *21*, 3586.
(32) Washington, A. L.; Strouse, G. F. *J. Am. Chem. Soc.* **2008**, *130*, 8916.
(33) Washington, A. L.; Strouse, G. F. *Chem. Mat.* **2009**, *21*, 2770.
(34) Gerbec, J. A.; Magana, D.; Washington, A.; Strouse, G. F. *J. Am. Chem. Soc.* **2005**, *127*, 15791.
(35) Kappe, C. O. *Angew. Chem., Int. Ed.* **2004**, *43*, 6250.
(36) Nuchter, M.; Ondruschka, B.; Bonrath, W.; Gum, A. *Green Chem.* **2004**, *6*, 128.
(37) Belton, D. J.; Deschaume, O.; Patwardhan, S. V.; Perry, C. C. *J. Phys. Chem. B* **2010**, *114*, 9947.
(38) Brinker, C. J. *J. Non-Cryst. Solids* **1988**, *100*, 31.
(39) Schaffer, C. L.; Thomson, K. T. *J. Phys. Chem. C* **2008**, *112*, 12653.
(40) Artaki, I.; Sinha, S.; Irwin, A. D.; Jonas, J. *J. Non-Cryst. Solids* **1985**, *72*, 391.
(41) Hayn, R. A.; Owens, J. R.; Boyer, S. A.; McDonald, R. S.; Lee, H. J. *J. Mater. Sci.* **2011**, *46*, 2503.